PHYSICAL REVIEW B **87**, 201403(R) (2013)

Valley-polarized massive charge carriers in gapped graphene

E. C. Peters,[1,*] A. J. M. Giesbers,[1,2,†] U. Zeitler,[3] M. Burghard,[1] and K. Kern[1,4]

[1]*Max Planck Institute for Solid State Research, Heisenbergstrasse 1, D-70569 Stuttgart, Germany*

[2]*Department of Applied Physics, Eindhoven University of Technology, 5600 MB Eindhoven, The Netherlands*

[3]*High Field Magnet Laboratory and Institute for Molecules and Materials, Radboud University Nijmegen, Toernooiveld 7, 6525 ED Nijmegen, The Netherlands*

[4]*Institute de Physique de la Matière Condensée, Ecole Polytechnique de Lausanne, CH-1015 Lausanne, Switzerland*

(Received 14 January 2013; revised manuscript received 9 April 2013; published 30 May 2013)

The lifting of the fourfold degeneracy of the zeroth Landau level in graphene under high magnetic fields has been the subject of numerous experimental studies, and attributed to various mechanisms such as pure spin splitting, spin splitting combined with subsequent valley splitting, or the formation of a quantum Hall insulator. Unexplored, however, is the influence of an energy gap on the quantum Hall effect (QHE) states in graphene. Here we demonstrate, using measurements of the magnetoresistance of graphene antidot lattices (GALs) in magnetic fields up to 30 T and temperatures between 2 and 100 K, that gap opening in these samples is accompanied by valley polarization and a change from linear to parabolic band structure at low carrier energies. The emergence of a massive character of the carriers profoundly alters the transport characteristics of the zeroth Landau level, which manifests itself in a linear increase of the activated gap with magnetic field. Furthermore, samples of the highest quality display spin splitting on top of the valley splitting, albeit of significantly smaller magnitude.

DOI: 10.1103/PhysRevB.87.201403 PACS number(s): 72.80.Vp, 72.20.Ee, 73.22.Pr, 73.43.Qt

I. INTRODUCTION

Graphene's remarkable electronic properties arise from its peculiar lattice structure with two different sublattices, which leads to a linear energy dispersion wherein the valence and conduction band meet at the charge neutrality point (CNP).[1] As a characteristic feature of graphene, its $N = 0$ Landau level (LL) is equally shared by electrons and holes, with the fourfold degeneracy originating from the spin and sublattice symmetry (pseudospin). High magnetic fields can lift the degeneracy,[2–4] which has mainly been ascribed to electron-electron interactions[4,5] or the Zeeman effect.[2,3,6,7] Recently, the issue of whether the symmetry breaking favors "spin-first, valley-later" splitting or vice versa[8] has attracted increasing attention. Preferential valley splitting could for example provide access to a valley Hall effect, wherein carriers in different valleys flow to opposite transverse edges upon application of an in-plane electric field. The valley Hall effect belongs to the same category of Berry-phase supported topological transport phenomena as its counterpart, the spin Hall effect.[9]

Despite the progress in exploring the zeroth LL of pristine graphene, only little is known about the impact of an energy gap on the LL splitting hierarchy in graphene. Addressing this question requires a method to reliably introduce a band gap.[10] One possible strategy is to introduce lateral confinement in the form of a graphene antidot lattice (GAL).[11] According to theory, GALs have a fundamental band gap that scales inversely with the neck width between the nanoholes, akin to graphene nanoribbons.[12–15] From the experimental side, a transport gap, whose magnitude increases with decreasing neck width,[16,17] has been observed, although unequivocal proof for the presence of a fundamental band gap has remained elusive so far.[18] Theory furthermore predicts that an isolated graphene antidot in a magnetic field causes breaking of the electron-hole symmetry in the individual valleys.[19] Here we present magnetotransport data acquired from GALs of different geometry, demonstrating that the antidot confinement potential opens a gap which induces a parabolic dispersion for electrons and holes. The associated valley-split lowest LLs are found to be attached to this parabolic, and accordingly the actual gap measured is composed of the zero-field gap plus the cyclotron energy.

II. EXPERIMENTAL RESULTS AND DISCUSSION

A. Experiment

An example of the investigated GALs, electrically contacted in Hall bar geometry, is displayed in Fig. 1(a). A series of pristine graphene and GAL devices were fabricated either on a Si/SiO_2 substrate or freely suspended, following a previously described procedure.[18] The CNP of the samples typically ranged between $V_{CNP} = 5$ and 20 V, while for the suspended flakes it was located close to zero gate voltage ($V_{CNP} = 0$ V) after current annealing. Electrical measurements were performed by standard ac lock-in techniques with an input impedance of 100 MΩ down to $T = 1.4$ K and under external magnetic fields up to 30 T. We investigated a total of 13 devices on 7 different substrates, with a maximum carrier mobility of 5.000 $cm^2/V\,s$ reached for GALs on SiO_2, and up to 20.000 $cm^2/V\,s$ for suspended devices.

B. Divergence of magnetoresistance

In Fig. 1(a) the magnetic field-dependent electrical resistance at the CNP and $T = 1.4$ K is depicted for nonstructured graphene and two different GALs with a nanohole spacing of 100 and 200 nm, respectively. The pristine graphene exhibits a monotonous positive magnetoresistance at low magnetic fields, most likely arising from spatial carrier mobility fluctuations.[20] Under higher B fields (>10 T), in the quantum Hall regime, the resistance increase becomes more pronounced, indicative of degeneracy lifting of the zeroth

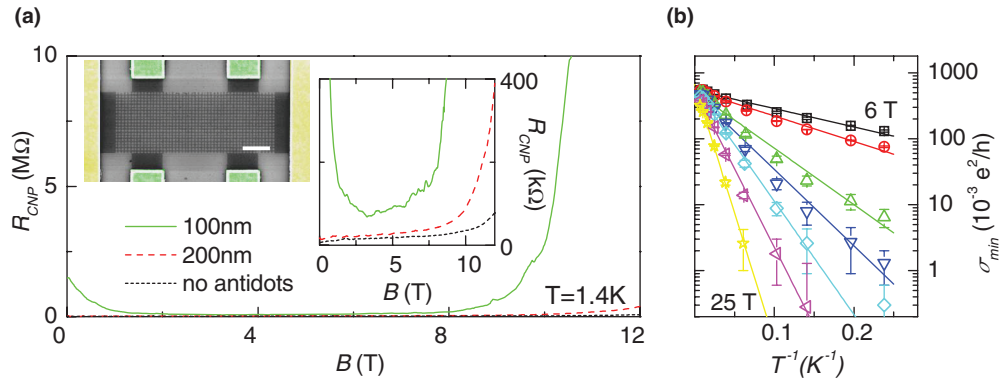

FIG. 1. (Color online) (a) Lateral four-probe magnetoresistance of GALs with 100 nm (solid green line) and 200 nm spacing (dashed red line), and a pristine graphene device (short dashed black line). Right inset: Zoom of the magnetoresistance in the main panel. Left inset: Scanning electron micrograph (scale bar is 1 μm) of a typical Hall bar device with 100 nm nanohole spacing. The current leads and Hall probe contacts are colored yellow and green, respectively. (b) Arrhenius plot of the conductivity at the CNP of the 100 nm spacing sample for magnetic fields between 6 and 25 T.

LL.[2–4] By comparison, the GAL with 100 nm nanohole spacing features a quasilinear negative magnetoresistance up to ∼1 T, ascribable to a change of the hopping probability between localized states in this regime.[18,21–23] At higher B fields, the sample displays a diverging, positive magnetoresistance. A similar behavior has been observed for several other 100 nm spacing samples, and also for the GAL with 200 nm nanohole spacing, albeit with a weaker resistance increase in the latter case. Figure 1(b) reveals that for the B field range between 6 and 25 T, the minimum conductivity of a 100 nm spacing GAL as a function of inverse temperature can be well fitted by the Arrhenius equation[24] $\sigma \propto \exp(-E_a/2k_BT)$, where E_a is the activation gap.

To further analyze the diverging magnetoresistance we explore the carrier concentration dependence of both the Hall and longitudinal resistance. The Hall resistance of a 100 nm spacing GAL device ($V_{\mathrm{CNP}} = 15.5$ V) is depicted in Fig. 2(a) as a function of the voltage $V = V_G - V_{\mathrm{CNP}}$, with the back gate voltage V_G. The resistance plateaus observed at $R_{xy} = \{\pm 2h/e^2, \pm 6\, h/e^2, \ldots\}$ corresponding to filling factors $\nu = \{\pm 2, 6, \ldots\}$ are characteristic of the LL pattern of pristine graphene. At temperatures above 30 K, there is a smooth zero transition of R_{xy} between the $\nu = -2$ and $\nu = +2$ plateaus, even at the highest B field (see data at 88 K). This behavior is similar to pristine graphene, and testifies a finite, equal density of electrons and holes near the CNP.[25] However, below 30 K, R_{xy} diverges at small charge carrier densities q, and does not cross zero anymore for magnetic fields above 10 T. The divergence of the Hall resistance follows a $(\pm 1/q)$ dependence away from the quantized $\nu = \pm 2$ plateaus, and occurs at higher absolute voltages $|V_G - V_{\mathrm{CNP}}|$ with increasing B field. Correspondingly, the longitudinal (σ_{xx}) and transverse (σ_{xy}) conductivity flatten into a zero plateau toward the CNP upon crossing from filling factor $\nu = -2$ to $\nu = +2$ [see Fig. 2(b)]. Close to the CNP no current could be detected within the digitalization limit, revealing the presence of an insulating state. The Hall data, taken together with the temperature dependent conductivity and diverging magnetoresistance, prove the presence of a fundamental energy gap in the GALs.

C. Valley-first splitting of the $N = 0$ LL

The Hall resistance data in Fig. 2(a) provide direct access to the electron and hole density via the inverse Hall coefficient

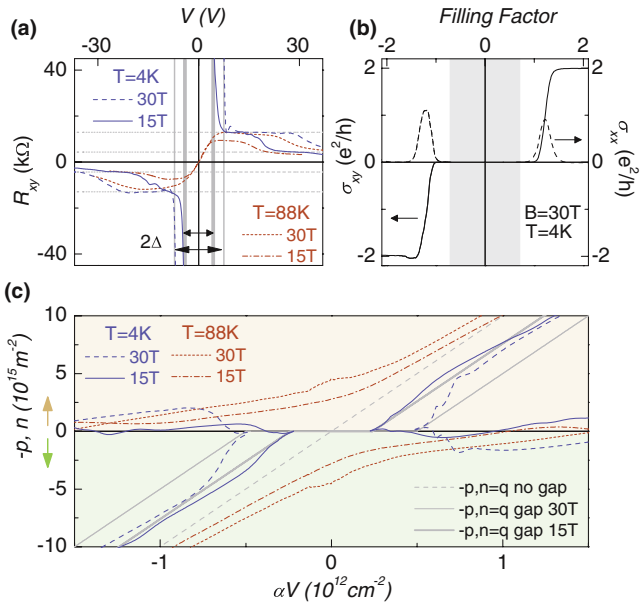

FIG. 2. (Color online) (a) Hall resistance measured at $V_{\mathrm{CNP}} = 15.5$ V for $T = 4$ K and $T = 88$ K, each at magnetic fields of $B = 15$ T and $B = 30$ T. For temperatures above the band gap ($T = 88$ K), the Hall resistance shows a smooth, monotonous zero crossing around the CNP. Below the band gap ($T = 4$ K), the Hall resistance diverges, while outside the insulating region the usual graphene QHE plateaus occur at filling factors $\nu = \{\pm 2, \pm 6, \pm 10, \ldots\}$ (dashed gray horizontal lines). (b) Longitudinal and transverse conductivity of the same sample. The shaded area indicates the insulating regime. (c) Concentration of electrons (positive values) and holes (negative values), as determined from the Hall data. At $T = 88$ K (dash-dotted red line $B = 15$ T; dashed red line $B = 30$ T) electrons and holes coexist at the CNP. At $T = 4$ K (solid blue line $B = 15$ T; dashed blue line $B = 30$ T), the gap region emerges. The three light gray curves (solid bold, solid fine, and dashed) are ideal curves representing pure electron or hole conduction outside the gap for different gap sizes.

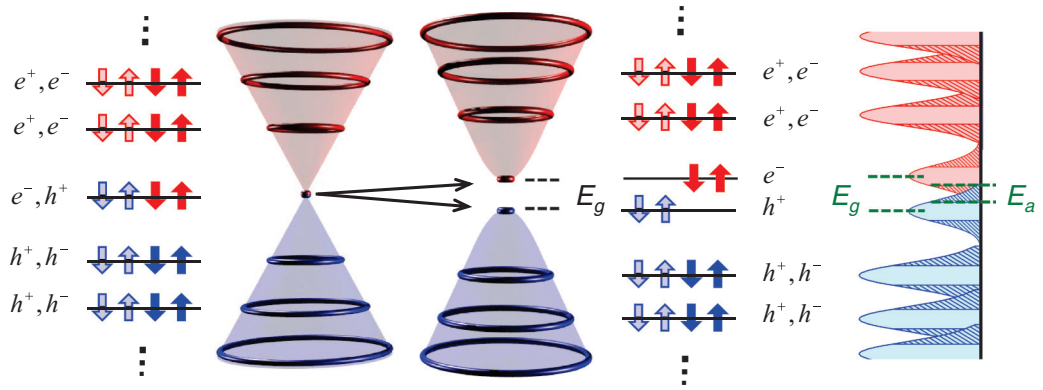

FIG. 3. (Color online) Schematic illustration of B-field induced splitting of the zeroth Landau level in the GALs, with concomitant transition from a linear to a parabolic dispersion close to the band edges. The resulting Landau level density of states displays an actual LL gap E_g which is distinguished from the activation gap E_a (both in dark green).

$1/R_H = B/R_{xy}$. For a semiconductor with two types of charge carriers, the densities are related to the Hall coefficient by[26]

$$\frac{1}{R_H} = \frac{e(n\mu_n + p\mu_p)^2}{n\mu_n^2 - p\mu_p^2}, \tag{1}$$

where n and p are the electron and hole density, and μ_n and μ_p are the corresponding mobilities. This simple two-carrier model is applicable to graphene despite the presence of electron-hole puddles since tunneling between the corresponding areas can occur.[25] In the present samples, the conductance is symmetric in charge carrier density around the CNP, and hence the condition of equal mobility is fulfilled ($\mu_p = \mu_n$). In case of a zero band gap, the total charge carrier density $q = n - p$ can be determined from $q = \alpha V$, with $\alpha = 8.5 \times 10^{10}$ cm^{-2} V^{-1} as the gate coupling constant for the 100 nm spacing sample. In Fig. 2(c) the resulting coexisting electron density $n = \frac{1}{2}[(n+p)+q]$ and (negative) hole density $-p = -\frac{1}{2}[(n+p)-q]$ around the CNP are plotted as a function of q. In the n-type regime ($q > 5 \times 10^{15}$ m^{-2}), electrons are the majority charge carriers approaching a density of $n = q$, while the hole density p approaches zero (vice versa for the p-type regime). At the CNP the carrier density is $n = p = 2.8 \times 10^{15}$ m^{-2} at $T = 88$ K and $B = 15$ T. Similar to pristine graphene,[25] the individual carrier density increases when the magnetic field is further increased since the degeneracy of the $N = 0$ LL is proportional to the B field, reaching $n = p = 4.5 \times 10^{15}$ m^{-2} at $B = 30$ T. Upon cooling to $T = 4$ K, the Hall resistance R_{xy} starts to diverge at the CNP, and at $B = 15$ T the zero crossing has vanished [see Fig. 2(a)], indicating that electrons and holes no longer coexist near the CNP. For higher magnetic fields, R_{xy} starts to rise from the $\nu = \pm 2$ plateaus already at higher gate voltage, evidencing a stronger $N = 0$ Landau level splitting $2\Delta q$ in the charge carrier density. This trend is mirrored in the charge carrier density plot [see Fig. 2(c)] by a shift of the asymptote from $\alpha V = \pm\Delta q = \pm 2.2 \times 10^{15}$ m^{-2} at $B = 15$ T to $\pm 4.6 \times 10^{15}$ m^{-2} at $B = 30$ T. Inside the insulating region $-\Delta q \leqslant \alpha V \leqslant \Delta q$, the equality $n = p = q = 0$ holds, while to the left ($\alpha V \leqslant -\Delta q$) the total charge carrier density is $q = \alpha V + \Delta q$, and, accordingly, the conduction is p type with $n = 0$ and $-p = q$. By comparison, to the right ($\alpha V \geqslant \pm\Delta q$) the total charge carrier density is $q = \alpha V - \Delta q$, resulting in n-type conduction with $p = 0$ and $n = q$.

Since valley-first splitting is a necessary and sufficient condition for the occurrence of a diverging Hall resistance,[25] it follows that the gap separates electrons and holes into two valley split $N = 0$ LLs, whereas the spin degeneracy is preserved, as illustrated in Fig. 3. Support for this conclusion derives from the fact that R_{CNP} depends only on the perpendicular B-field component rather than the total B field (see Fig. 4). In these measurements, the sample was rotated out-of plane by an angle θ relative to the sample orientation perpendicular to the external field. As exemplified for constant total fields of $B_{\mathrm{tot}} = 1$, 6, 12, and 14 T, the angle-dependent resistance at these magnetic fields coincides with the values recorded at zero angle, where $B_{\mathrm{tot}}\ (\theta = 0^\circ) = B_{\mathrm{perp}}\ (\theta)$. Moreover, the minimum resistance remains unchanged upon keeping the perpendicular field constant at different values of B_{tot} (see inset), with corresponding angle θ [$B_{\mathrm{perp}} = B_{\mathrm{tot}} \cos(\theta)$]. Both data sets confirm that the gap is not related to Zeeman splitting.

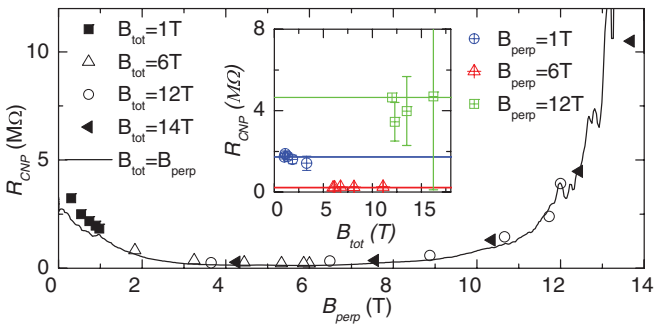

FIG. 4. (Color online) Four-terminal measurements on a 100 nm spacing device in tilted magnetic fields at $T = 4$ K. Data were taken at angles $\theta = 0^\circ$, 15°, 30°, 45°, 60°, and 75°. The solid line represents the resistance at the CNP as a function of perpendicular field $B_{\mathrm{perp}} = B_{\mathrm{tot}} \cos(\theta)$ at $\theta = 0^\circ$ for a 100 nm spacing GAL device. At $\theta = 0^\circ$ (solid line) the resistance at the CNP shows a negative magnetoresistance at small fields and a pronounced positive magnetoresistance at higher fields. In the inset the total field is kept constant while the perpendicular field changes. Here the resistance remains at the zero angle value (solid lines) within the error bars.

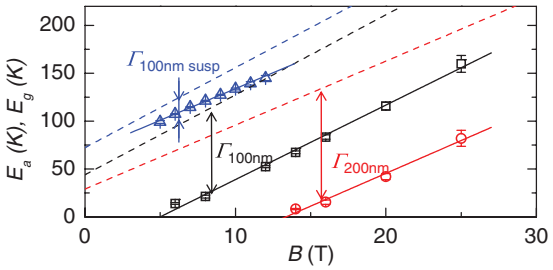

FIG. 5. (Color online) Magnetic field dependent activation gaps for the 100 nm (black squares), 200 nm (red circles), and 100 nm suspended (blue triangles) spacing samples, with the full lines representing linear fits. The dashed lines correspond to the calculated gap values E_g (see main text), while the arrows indicate the LL broadening Γ.

D. Introduction of a parabolic dispersion at small energies

The overall charge transport characteristics can be consistently explained on the basis of a small band gap introduced by the antidot lattice.[13–15] Under an applied magnetic field, the E_a values extracted from the temperature dependence [see Fig. 1(b)] exhibit a close-to-linear dependence on the magnetic field, as demonstrated by Fig. 5. Band structure calculations indicate that the gap opening in GALs is accompanied by the emergence of a parabolic energy dispersion in vicinity of the gap[13–15] (see Fig. 3). In the QHE regime, the two levels originating from the $N = 0$ LL reside within this parabolic dispersion region, whereas the higher ($N \neq 0$) LLs remain in the linear dispersion regime and are hence expected to mirror the LL structure of pristine graphene. The parabolic dispersion regime can be described by

$$E(k) = \pm\left(\frac{\hbar^2 k^2}{2m} + \frac{E_g^0}{2}\right), \tag{2}$$

where m is the mass, E_g^0 is the zero-field band gap originating from the antidot lattice, and the $\pm$ sign accounts for electrons and holes, respectively. The energy of the two $N = 0$ LLs is therefore given by

$$E_\pm = \pm\tfrac{1}{2}\left(\hbar\omega_c + E_g^0\right), \tag{3}$$

with the cyclotron frequency $\omega_c = eB/m$. The magnetic field dependent band gap is thus given by $E_g = E_+ - E_- = \hbar\, eB/m + E_g^0$, where $m = m_{\text{eff}} m_e$, with m_e as the free electron mass. The LL energies can be related to the experimentally accessible gate voltages by rewriting Eq. (3) in terms of the gate voltage by using $V = q/\alpha = k^2/2\pi\alpha = Em/\pi\hbar^2\alpha$, which leads to

$$V_\pm = \pm\frac{1}{2}\left(\frac{eB}{\alpha\pi\hbar} + \frac{m_{\text{eff}} m_e}{\alpha\pi\hbar^2} E_g^0\right), \tag{4}$$

where $V = V_G - V_{\text{CNP}}$. Thus, in a parabolic dispersion V depends linearly on the magnetic field. Note that in the linear dispersive regime, the gate voltage positions of the $N \neq 0$ LLs also depend linearly on B field. This is apparent from the conversion of $E = \text{sqrt}(2e\hbar v_F^2 B|N|)$ to gate voltage positions using $V = q/\alpha = E^2/(\pi\hbar^2 v_F^2 \alpha)$, which yields $V_\pm = \pm 2eB|N|/(\pi\hbar\alpha)$.

The B-field dependent LL positions for the 100 nm spacing sample are visualized in the LL fan diagram of Fig. 6(a), where the first derivative of the inverse Hall resistance $-d(1/R_{xy})/dV$ is plotted as a function of both gate voltage and magnetic field. To the right-hand side, line cuts are provided for the inverse Hall resistance as well as its derivative at $B = 30$ T. The maxima within the green regions in the fan diagram mark the transitions from one QHE plateau to the following, and therefore represent the center of a LL. The black lines are fits to Eq. (4), which yield an effective mass $m_{\text{eff}} = 0.08$ and a zero-field gap $E_g^0 = 22.0$ K. The latter value is in good agreement with the estimated gap size of $E_g^0 \approx 15$ K for similar GALs at zero magnetic field.[23] A gate coupling factor of $\alpha = 8.5 \times 10^{10}$ cm^{-2} V^{-1} was extracted from the slope of the higher LLs (red dash-dotted lines). The slightly increased α results most likely from inhomogeneous electric field effects,

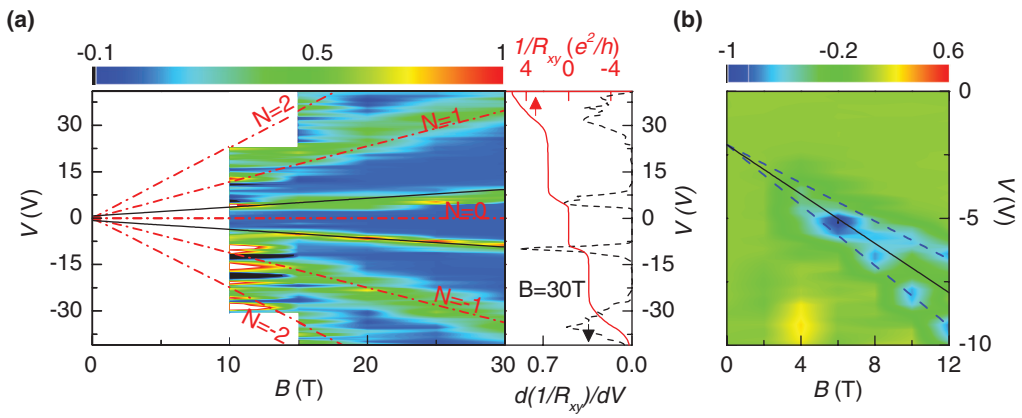

FIG. 6. (Color online) (a) Fan diagram displaying the first derivative of the inverse Hall resistance as a function of gate voltage and magnetic field for the 100 nm spacing sample. The blue regions correspond to the QH plateaus, the green regions to transitions between the plateaus at the LL positions. The red dashed lines represent the LLs in pristine graphene ($V \propto E^2$). The solid black lines represent the split $N = 0$ LL assuming a parabolic dispersion ($V \propto E$) in combination with a finite zero-field gap E_g^0. (b) Fan diagram of the suspended 100 nm spacing sample. The solid line indicates the position of the lowest LL, and the two dashed blue lines correspond to values calculated by taking the Zeeman term $\pm g^* m_{\text{eff}} eB/4\alpha\pi\hbar$ into account.

analogous to observations made on graphene nanoribbons.[27] In the same manner, values of $E_g^0 = 14.5$ K, $\alpha = 7.2 \times 10^{10}$ cm^{-2} V^{-1}, and $m_{\rm eff} = 0.10$ were obtained for the 200 nm spacing sample, and $E_g^0 = 33.0$ K, $\alpha = 5.0 \times 10^{10}$ cm^{-2} V^{-1}, and $m_{\rm eff} = 0.08$ for the suspended 100 nm spacing sample.

Combining the extracted values of $m_{\rm eff}$ and E_g^0 with Eq. (3) provides the B-field dependent gap between the two $N = 0$ LL center positions. In Fig. 5 this actual LL gap (dashed lines) is compared to the activation gaps (symbols). Since the activation gap is the distance between the mobility edges of the two broadened LLs, the difference between the activation gap and the actual gap corresponds to the LL broadening (see right part of Fig. 3). The extent of the LL broadening differs depending on the amount of disorder.[28,29] From the plot, the LL broadening is estimated to be $\Gamma = (90 \pm 10)$, (120 ± 10), and (30 ± 10) K for the 100, 200, and suspended 100 nm spacing sample, respectively. The latter broadening is appreciably smaller than the value of ∼100 K reported for pristine (nonsuspended) graphene at low temperatures.[30] It is furthermore noteworthy that a linear instead of parabolic energy dispersion could not account for the observed magnetic field behavior. In fact, this would result in a quite weak, square-root-like dependence of the energy gap on the B field,[1] such that reaching the measured LL positions would require an unrealistically big hypothetical gap of 1800 K at 20 T.

E. Additional spin splitting

In the samples of highest quality, we could also detect signatures of additional spin splitting associated with the $N = 0$ LL, specifically a $\nu = 1$ plateau appears at $R_H = h/e^2$. It is best visible in the LL fan plots of the suspended 100 nm spacing sample above 6 T, as exemplified by Fig. 6(b) showing a zoom into the hole regime of the sample. The spin splitting can be accounted for by the parabolic dispersion near the Dirac point [Eq. (3)] complemented by a Zeeman term $\pm g^* \mu_B B$, with g^* as the effective electron g factor, which leads to an additional term $\pm g m_{\rm eff} eB/4\alpha\pi\hbar$ in Eq. (4). The solid line in Fig. 6(b) represents the fit to Eq. (4) without spin splitting, whereas the dashed lines include spin splitting. As both fits yield identical E_g^0 and $m_{\rm eff}$ the g factor remains the only free fit parameter. On this basis, one obtains a g factor of $g^* = 6$ for the 200 nm GAL and $g^* = 5$ for the 100 nm suspended sample. These quite large values might be explained by electron-electron exchange interactions, in analogy to the 2D gas in semiconductor heterojunctions:[31,32]

$$E_{\rm ex}^0 = \left(1 - \frac{g}{g^*}\right)\sqrt{2\pi}\Gamma. \tag{5}$$

When spin splitting is included, the estimated LL broadening decreases to $\Gamma = 60$ K for the 200 nm spacing sample, and $\Gamma = 20$ K for the suspended 100 nm spacing sample, as derived from the field at which the spin splitting becomes visible. This results in respective exchange energies of $E_{\rm ex}^0 = 100$ K and $E_{\rm ex}^0 = 30$ K, which correspond well with $E_{\rm ex}^0 = 130$ K reported for pristine graphene.[30]

III. CONCLUSION

The observed QH insulator behavior points toward valley-first splitting in the GALs provided that the charge carriers would be associated with different valleys in the lowest LL, similar to the case of pristine graphene. Due to the possibility of sizable intervalley scattering, however, the situation might be more complicated than for unstructured graphene, such that further studies are needed to determine the effect of the periodic nanohole array on the quasiparticle properties. From an application perspective, valley-first splitting could be exploited for graphene-based valleytronic devices such as gate-tuned valley filters or beam splitters.[33,34] To this end, GAL devices of improved mobility (e.g., by use of BN) would be highly beneficial. In addition, the emergence of a massive character of the charge carriers is relevant for all graphene semiconductor applications that rely upon a band gap introduced by spatial confinement, like in, e.g., nanoribbons. In fact, the introduction of a charge carrier mass at low carrier densities might alter other properties unique to graphene.

ACKNOWLEDGMENTS

Part of this work has been supported by EuroMagNET under EU Contract RII3-CT-2004-506239 and by the Foundation for Fundamental Research on Matter (FOM), A.J.M.G. acknowledges financial support from the Netherlands Organization for Scientific Research (NWO).

*Corresponding author: e.c.peters@fkf.mpg.de

†a.j.m.giesbers@tue.nl

[1] K. S. Novoselov, A. K. Geim, S. V. Morozov, D. Jiang, M. I. Katsnelson, I. V. Grigorieva, S. V. Dubonos, and A. A. Frisov, Nature (London) **438**, 197 (2005).

[2] A. J. M. Giesbers, L. A. Ponomarenko, K. S. Novoselov, A. K. Geim, M. I. Katsnelson, J. C. Maan, and U. Zeitler, Phys. Rev. B **80**, 201403(R) (2009).

[3] Y. Zhang, Z. Jiang, J. P. Small, M. S. Purewal, Y.-W. Tan, M. Fazlollahi, J. D. Chudow, J. A. Jaszczak, H. L. Stormer, and P. Kim, Phys. Rev. Lett. **96**, 136806 (2006).

[4] J. G. Checkelsky, L. Li, and N. P. Ong, Phys. Rev. Lett. **100**, 206801 (2008).

[5] M. O. Goerbig, R. Moessner, and B. Douçot, Phys. Rev. B **74**, 161407(R) (2006).

[6] D. A. Abanin, K. S. Novoselov, U. Zeitler, P. A. Lee, A. K. Geim, and L. S. Levitov, Phys. Rev. Lett. **98**, 196806 (2007).

[7] E. Shimshoni, H. A. Fertig, and G. Venketeswara Pai, Phys. Rev. Lett. **102**, 206408 (2009).

[8] A. F. Young, C. R. Dean, L. Wang, H. Ren, P. Cadden-Zimansky, K. Watanabe, T. Taniguchi, J. Hone, K. L. Shepard, and P. Kim, Nat. Phys. **8**, 550 (2012).

[9] S. Murakami, N. Nagaosa, and S.-C. Zhang, Science **301**, 1348 (2003).

[10] F. Guinea, M. I. Katsnelson, and A. K. Geim, Nat. Phys. **6**, 30 (2010).

[11] T. G. Pedersen, C. Flindt, J. Pedersen, N. A. Mortensen, A.-P. Jauho, and K. Pedersen, Phys. Rev. Lett. **100**, 136804 (2008).
[12] Y.-W. Son, M. L. Cohen, and S. G. Louie, Phys. Rev. Lett. **97**, 216803 (2006).
[13] H. Jippo, M. Ohfuchi, and C. Kaneta, Phys. Rev. B **84**, 075467 (2011).
[14] J. A. Furst, J. G. Pedersen, C. Flindt, N. A. Mortensen, M. Brandbyge, T. G. Pedersen, and A.-P. Jauho, New J. Phys. **11**, 095020 (2009).
[15] F. Ouyang, S. Peng, Z. Liu, and Z. Liu, ACS Nano **5**, 4023 (2011).
[16] T. Shen, Y. Q. Wu, M. A. Capano, L. P. Rokhinson, L. W. Engel, and P. D. Ye, Appl. Phys. Lett. **93**, 122102 (2008).
[17] J. Eroms and D. Weiss, New J. Phys. **11**, 095021 (2009).
[18] A. J. M. Giesbers, E. C. Peters, M. Burghard, and K. Kern, Phys. Rev. B **86**, 045445 (2012).
[19] J. G. Pedersen and T. G. Pedersen, Phys. Rev. B **85**, 035413 (2012).
[20] J. S. Hu and T. F. Rosenbaum, Nat. Mater. **7**, 697 (2008).
[21] W. Schirmacher, Phys. Rev. B **41**, 2461 (1990).
[22] U. Sivan, O. Entin-Wohlman, and Y. Imry, Phys. Rev. Lett. **60**, 1566 (1988).
[23] E. C. Peters, A. J. M. Giesbers, and M. Burghard, Phys. Status Solidi B **249**, 2522 (2012).
[24] B. I. Shklovskii and A. L. Efros, *Springer Series in Solid-State Sciences*, edited by M. Cardona, P. Fulde, and H.-J. Queisser, Vol. 45 (Springer, Berlin, 1984).
[25] S. Wiedmann, H. J. van Elferen, E. V. Kurganova, M. I. Katsnelson, A. J. M. Giesbers, A. Veligura, B. J. van Wees, R. V. Gorbachev, K. S. Novoselow, J. C. Maan, and U. Zeitler, Phys. Rev. B **84**, 115314 (2011).
[26] K. Seeger, *Semiconductor Physics, An Introduction* (Springer, Berlin, 1997), p. 61.
[27] A. Behnam, A. S. Lyons, M. H. Bae, E. K. Chow, S. Islam, C. M. Neumann, and E. Pop, Nano Lett. **12**, 4424 (2012).
[28] A. J. M. Giesbers, U. Zeitler, M. I. Katsnelson, L. A. Ponomarenko, T. M. Mohiuddin, and J. C. Maan, Phys. Rev. Lett. **99**, 206803 (2007).
[29] C. H. Yang, F. M. Peeters, and W. Xu, Phys. Rev. B **82**, 075401 (2010).
[30] E. V. Kurganova, H. J. van Elferen, A. McCollam, L. A. Ponomarenko, K. S. Novoselov, A. Veligura, B. J. van Wees, J. C. Maan, and U. Zeitler, Phys. Rev. B **84**, 121407(R) (2011).
[31] Th. Englert, D. C. Tsui, A. C. Gossard, and Ch. Uihlein, Surf. Sci. **113**, 295 (1982).
[32] R. J. Nicholas, R. J. Haug, K. v. Klitzing, and G. Weimann, Phys. Rev. B **37**, 1294 (1988).
[33] A. Rycerz, J. Tworzydło, and C. W. J. Beenakker, Nat. Phys. **3**, 172 (2007).
[34] J. L. Garcia-Pomar, A. Cortijo, and M. Nieto-Vesperinas, Phys. Rev. Lett. **100**, 236801 (2008).